Hindawi
International Journal of Photoenergy
Volume 2021, Article ID 5556441, 12 pages
https://doi.org/10.1155/2021/5556441

Research Article

Preparation and Characterization of Nickel and Aluminum-Codoped SnO_2 Thin Films for Optoelectronic Applications

El Mahdi Bouabdalli,[1,2] **Mohamed El Jouad**,[1] **Taoufik Garmim**,[2] **Samira Touhtouh**,[1] **Ahmed Louardi**,[2,3] **Mohamed Monkade**,[2] **and Bouchaib Hartiti**[4]

[1]*Laboratory of Engineering Sciences for Energy (LabSIPE), National School of Applied Sciences, Chouaib Doukkali University, El Jadida 24000, Morocco*
[2]*Laboratory of Condensed Matter Physics (LPMC), Department of Physic, Faculty of Sciences, Chouaïb Doukkali University, El Jadida 24000, Morocco*
[3]*Laboratory of Industrial Techniques, Department of Industrial Engineering, Faculty of Sciences and Techniques, Sidi Mohamed Ben Abdellah University, Fez, Morocco*
[4]*MAC&PM Laboratory, ANEPMAER Group FSTM, Hassan II Casablanca University, B.P 146 Mohammedia, Morocco*

Correspondence should be addressed to El Mahdi Bouabdalli; bouabdalli.e@ucd.ac.ma

Received 11 February 2021; Revised 25 June 2021; Accepted 7 August 2021; Published 10 September 2021

Academic Editor: Paolo Fornasiero

In this study, the coating technique was used to prepare thin layers of nickel and aluminum-codoped tin oxide (SnO_2: Ni; Al). This study is aimed at exploring the influence of aluminum (Al) dopant on the structural, optical, and electrical properties of the elaborated films. X-ray diffraction (XRD) studies discovered that all deposited films (Ni-doped and Al-Ni-codoped SnO_2) were polycrystalline with tetragonal (quadratic) structure and exhibited [110] preferential orientation. The optical measurements exposed that all prepared films have presented good transparency. The transmittance of Ni-Al-codoped SnO_2 thin films in the visible and near-infrared regions varied between 80% and 90%; this was dependent on the concentration of dopant. The band gap was determined via the equation related to the absorption coefficient. It was deduced that the optical band gap values of thin films gradually decreased from 4.084 eV to 3.991 eV, as an effect of Al content. In addition, it was concluded that the thickness values of the films pass from 571.374 nm to 694.036 nm as an effect of Al content. Moreover, the extinction coefficient decreases with the wavelength in the UV region and then varies slightly towards longer wavelengths. Moreover, the electrical resistivity was determined using the four-point probe; it was determined that the electrical resistivity decreases from $1.35 \times 10^3 (\Omega \cdot \mathrm{cm})$ to $0.14 \times 10^3 (\Omega \cdot \mathrm{cm})$ with aluminum concentration increasing from 0 at. % to 7 at. %. The elaborated films of SnO_2 codoped with Ni and Al present were highly transparent; therefore, these thin layers look promising in the use of the window layer in PV solar cells.

1. Introduction

In the recent years, a lot of studies aimed at transparent conductive oxides (TCOs) were conducted; this included tin dioxide (SnO_2), zinc oxide (ZnO), indium oxide (In_2O_3), iron oxide (Fe_2O_3), and titanium oxide (TiO_2). These studies refer to a class of materials, which present the visible wavelength range, high optical transparency, and high reflectance in the infrared (IR) one with good electrical conductivity of nearly semimetallic regime. These optical and electrical properties make them suitable for several applications such as photocatalysis [1–5], liquid crystal displays [6], photothermal converters [7], transparent electrodes in solar cells [8–10], flat panel displays [11], light-emitting diodes [12], heated mirrors [13], gas sensors [14, 15], and other optoelectronic devices [16–18]. In this work, we will be presenting tin oxide SnO_2 known under the name of cassiterite in natural state, which is crystallized in the tetragonal crystalline structure

[7], belonging to the P42/mnm space group [19]. It is an n-type semiconductor [20, 21] and is the first transparent conductor widely marketed. In addition, it has a large band gap energy value varying between 3.6 and 4 eV [7, 16, 19]. Due to its properties such as low electrical resistivity, high optical transmittance [12, 21], and the big reflectivity in the infrared region, it can be used as, although anode in lithium-based batteries, a conductive electrode of thin layers of photovoltaic cells. The SnO_2 thin layers have been extensively prepared by employing different procedures like dual-beam pulsed laser deposition (DB-PLD) [22], spray pyrolysis [23], magnetron sputtering [24], molecular beam epitaxy (MBE) [25], and sol-gel method [26], which will be used with the spin coating to prepare our thin films; the reason this was chosen was because of its several advantages: its simplicity, low cost, and its ability to generally obtain uniform films with good adherence and reproducibility [27]. Until now, impurities for doping SnO_2 thin films have been applied by other researchers such as fluorine (F), antimony (Sb), copper (Cu), nickel (Ni), cobalt (Co), aluminum (Al), and Indium (In) [28–34].

The review of the literature revealed that SnO_2 doped with metal elements and followed by an annealing process [16] could give birth to the ideal electronic device where the crystalline, electrical conductivity, and morphological properties of doped SnO_2 layers are improved compared to the corresponding undoped layers and more of other TCO films [12, 14, 35–37]. In this context, the most important parameter that improves and significantly influences the electrical and optical properties is the doping with different metals, which have been mentioned previously. Moreover, many types of research for the modification of band gap are possible also with the doping of different transition metal cations that we have reported before. Among all metal cations, Ni has prominence due to its grain growth inhibition in the SnO_2 matrix [38]. In addition, the nickel (Ni) dopant in SnO_2 showed a decreasing particle size and to be improving the luminescent emission of the SnO_2, and it conducted a decrease in the band gap, particle size, and crystallinity. [39]. Furthermore, the Al^{3+} radius is equal to 0.54 Å, which is smaller than that of Sn^{4+} (0.71 Å). Therefore, Al ions can be substituted at the Sn^{4+} site in the SnO_2 system. Substitution of Al in the position of Sn^{4+} creates oxygen vacancies due to charge imbalance generating free electrons in the conduction band [40, 41]. Therefore, Al-doping slightly changes the nature of chemical bonding in its neighborhood. It becomes more ionic due to an increase of both positive and negative atomic charges of Sn and O atoms, respectively [42].

To our knowledge, the study of the properties of Ni- and Al- codoped SnO_2 thin films has not been mentioned in previous literature. Because of this limitation, in this paper, we have investigated the structural, optical, and electrical properties of SnO_2 thin films doped at 2% of Ni and x% of Al elaborated by spin coating.

2. Materials and Methods

2.1. Preparation of the Thin Films by a Sol-Gel Spin Coating Technique. The Ni-doped and Ni-Al-codoped SnO_2 thin films have been prepared by the sol-gel spin coating (SGSC) technique. Analytical reagent grade chemicals, such as ethanol, 2-methoxyethanol (ME), hydrochloric acid (HCl), tin chloride dehydrate ($SnCl_2$, $2H_2O$), nickel chloride ($NiCl_2$), and aluminum chloride ($AlCl_3$), were used as starting materials without any further purification. Firstly, SnO_2 (1 M) was prepared by dissolving tin chloride dehydrate ($SnCl_2{\cdot}2H_2O$) in 50 ml ethanol. Secondly, we have added a little hydrochloric acid (10^{-3} ml) [43], which ensures the maximum dissolution of $SnCl_2{\cdot}2H_2O$ solvent, and 2-methoxyethanol ($C_3H_8O_2$) which stabilizes the viscosity of the solution on the glass substrates. The mixture was well stirred by a magnetic agitator at room temperature for 20 minutes. Nickel chloride ($NiCl_2$) was then added into the solution as a dopant source with a ratio of $[Ni^{+2}]/[Sn^{+4}] = 2$ %. A magnetic agitator for 20 min also agitated this solution until it became homogeneous. Then, aluminum chloride ($AlCl_3$) was also added to the solutions as a second dopant with different concentrations divided in the ratio of $[Al^{+3}]/[Sn^{+4}]$ which was varied from 1 to 7 at. %. The glass substrates were cleaned in ethanol and acetone using an ultrasonic cleaner. The coating solution was deposited on the glass substrate (Corning 2947), which was rotating at 2500 rpm for 30 seconds. Then, the films were dried at 120°C while 10 min to eliminate the organic residues. This process of spin coating and drying was repeated ten times to obtain a layer with significant thickness. Finally, the obtained thin films were then annealed at the temperature of 500°C in a programmable furnace for 1 h at the rate of $2^{\circ}C{\cdot}min^{-1}$ to obtain the desired layers. Figure 1 illustrates the detailed schematic representation of the experimental sol-gel spin coating procedure as reported in [44].

2.2. Characterization. The crystalline structures of the Ni-doped and Al-Ni-codoped SnO_2 thin films were determined using an X-ray diffractometer (XPERT-PRO) by using CuKα radiation (CuKα = 0.15406 nm) with 2θ between 10° and 70°. The study of the optical properties of tin oxide thin films was carried out using a SHIMADZU 3101 PC UV-VIS-NIR spectrophotometer, being the spectral range extending over a range of 220 nm to 2400 nm. This nondestructive method consisted of recording the experimental spectral transmittance of the layers as a function of the wavelength and makes it possible to determine the value of the energy of the forbidden band or optical gap (E_g) of the layer (characteristics of a semiconductor), the refractive index of thin layers, and their thicknesses. The electrical resistivity measurements in the thin films were studied with a four-probe setup under normal conditions and at room temperature, using a JANDEL model RM3 digital multimeter. The thickness measurements of the thin films studied have been made by cross-sectional scanning electron microscopy (SEM).

3. Results and Discussion

3.1. Structural Properties. In order to study the effect of Al concentration on the structural properties of Al-Ni-codoped SnO_2 thin films, XRD analysis of the samples was performed. The obtained patterns are illustrated in

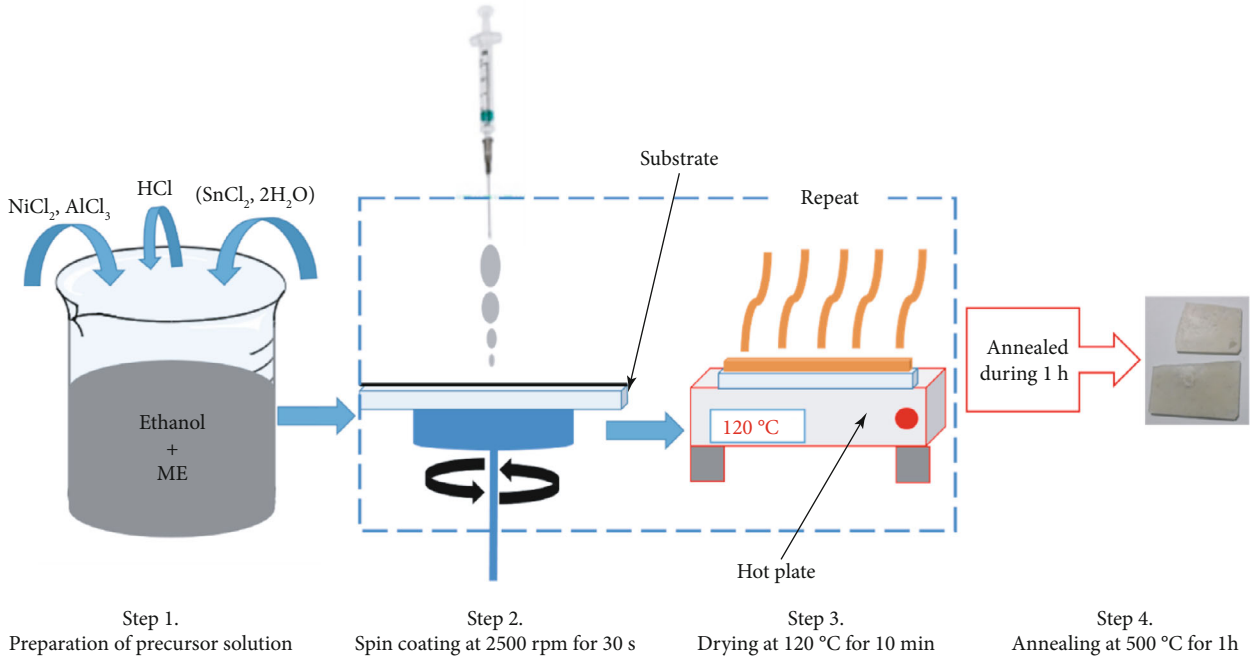

Figure 1: Schematic presentation of the experimental procedure of sol–gel spin coating.

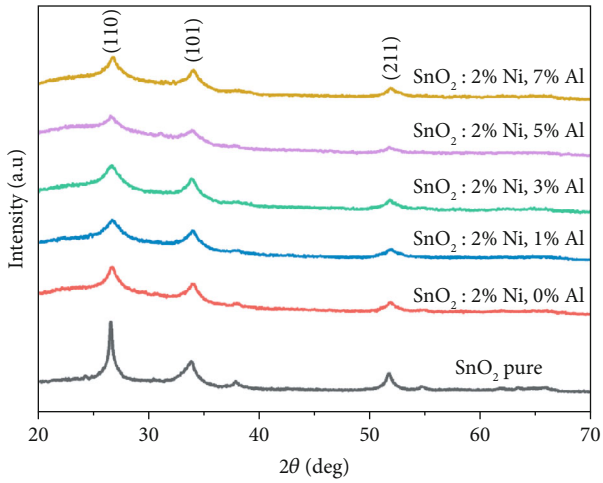

Figure 2: X-ray diffraction patterns of Al-Ni-codoped SnO_2 thin films with various aluminum-doping concentrations (0%, 1%, 3%, 5%, and 7%).

Figure 2. As revealed in Figure 2, the diffraction peaks were observed at $2\theta = 26.71^{\circ}$, 34.01°, and 51.94° which correspond, respectively, to the reticular planes (110), (101), and (211). It is interesting to note that all peaks of X-ray diffraction have the same peaks as the undoped SnO_2 sample. The prepared samples have the (110) diffraction peak as the most intense one, indicating that the (110) peak is the preferential growth direction [45] and has the (101) and (211) minor diffraction peaks reflecting the polycrystallinity of the structure of the undoped layers, which is in good agreement with the data from the JCPDS reference file (N°, 41-1445) which confirm the tetragonal cassiterite (rutile) structure crystal of our films [46]. The results explicate that Ni and Al incorporation does not change the tetragonal rutile-type structure of SnO_2.

No characteristic peaks of impurities were observed within the diffraction pattern of the samples, indicating that aluminum was substitutionally incorporated into the SnO_2 lattice. With the increase of the concentration of aluminum, the intensity of the peaks reduces. This can be explained by a disorder caused by the precipitation of aluminum in the grain boundaries. In addition, the diffraction peaks became broader due to crystallite size reduction.

The structural strain can be one of the most decisive negative factors, which consecutively affect the crystalline structure. The slight shift of the peak diffraction (110) of the Al-Ni-codoped SnO_2 thin films has resulted in the created structural strain associated with Al doping, which is calculated by the following formula [47]:

$$\varepsilon_{str} = -\Delta\theta_{hkl} \frac{1}{\text{tang}(\theta_{hkl})}, \quad (1)$$

where ε_{str} is the structural strain; $\Delta\theta_{hkl}$ is the width at half height expressed in radians (it is calculated compared to SnO_2 taken as origin); and θ_{hkl} is the diffraction angle.

Figure 3 displays the structural strain of Ni-doped and Al-Ni-codoped SnO_2 films as a function of the aluminum concentration. We can see that the structural strain of the prepared films is decreasing slightly when the aluminum concentration goes from 0 to 3 at. % Al indicates that the Al^{3+} ions enter the lattice both substitutionally and interstitially. When the concentration of aluminum increases, 5 at. % Al, the structural strain of the prepared films also increases. This growth results in deterioration and deformation in the SnO_2 crystal lattice structure. More particularly, this one is explained by the substitution of Sn^{+4} ion by that of Al^{+3} because of its weak ionic radius (0.054 nm) compared

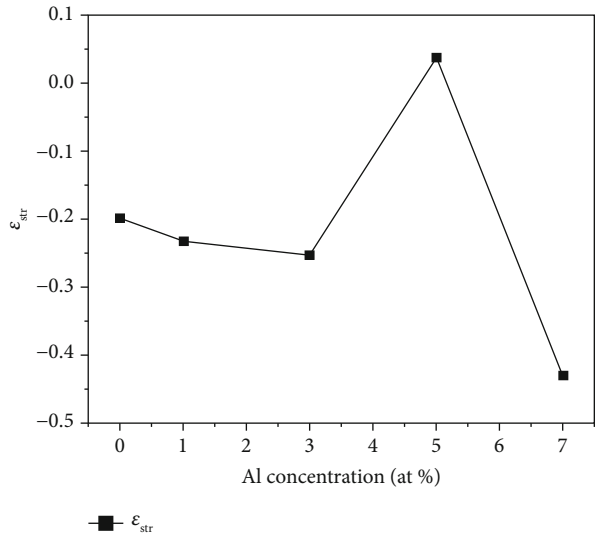

Figure 3: The structural strain of SnO_2 thin films codoped with Al-Ni as a function of the aluminum concentration.

to that of Sn^{+4} (0.071 nm); it decreases rapidly when the aluminum concentration exceeds 5 suggesting that most of the Al^{3+} ions incorporated in the lattice segregate in the grain boundaries. The lattice parameters "a" and "c" of the unit cell are calculated from the peak positions using the formula of the tetragonal system (equation (2)) [48]. The values are found to be $a = 4.7383$ Å and $c = 3.1866$ Å, which are close to those published in the literature [49].

$$d_{\text{hkl}} = \frac{a}{\sqrt{h^2 + k^2 + (a^2/c^2)l^2}}, \tag{2}$$

where d_{hkl} is the interplanar distance, (hkl) are the Miller indexes, and "a" and "c" are the lattice constants.

The modification of the lattice parameters as the content of aluminum can be found in Table 1. There is a slight decrease of " a" lattice parameters for all doping of aluminum in comparison with the lattice parameters of SnO_2 pure. It may be due to deformations which are produced by a weak compression in the crystal due to the substitution of ions Sn^{+4} of the largest ionic radius (0.71 Å) by the ions Al^{+3} of the low ionic radius (0.54 Å). This result is a good agreement with the previous studies in the literature [49].

The preferred orientations of the Al-Ni-codoped SnO_2 thin films are evaluated by the texture coefficient (T_C), calculated from the X-ray data using the well-known formula [50]:

$$T_C(\text{hkl}) = \frac{I(\text{hkl})/I_0(\text{hkl})}{(1/N)\sum_{\text{hkl}} I(\text{hkl})/I_0(\text{hkl})}, \tag{3}$$

where T_C (hkl) is the texture coefficient of the (hkl) plane, I is the measured or normalized intensity, I_0 is the corresponding standard intensity given in JCPDS data [46], and N is the number of reflections. The preferred orientation of the film will be the (hkl) plane for the higher value of T_C (hkl). Figure 4 presents T_C (hkl) values calculated (as seen in Table 1) from the above equation for the reflections (110) and (101) of the tetragonal Al-Ni-codoped SnO_2 thin films at the examined doping range. For codoped samples, it is noted that at the aluminum rate equal to 3 at. % Al, the (110) diffraction peak has the highest texture coefficient.

The average crystallite size (D) of the Al-Ni-codoped SnO_2 thin films is estimated from the X-ray diffraction patterns using the Scherrer formula [51]:

$$D = \frac{k\lambda}{\beta \cos(\theta)}, \tag{4}$$

where D is the average crystallite size, λ is the X-ray wavelength of incident CuKα radiation ($\lambda = 1.5418$ Å), k is the shape factor ($k = 0.9$), θ is the Bragg angle of the intense diffraction peak (110), and β is the experimental full-width at half-maximum of the (110) plane.

Using the average crystallite size values, the dislocation density (δ_{dis}), defined such as the length of dislocation lines per volume unit of the crystal, was calculated by employing the standard Williamson and Smallman formula [29]:

$$\delta = \frac{1}{D^2}. \tag{5}$$

The results of the crystallite size (D) and the dislocation density (δ_{dis}) are presented in Table 2. We observe a slight increase in the crystallite size as an aluminum concentration increases from 0 to 7 at. % in comparison with that of thin-film SnO_2 pure, except at 3%, which has a minimum crystallite size of 2.37 nm. The increase of the crystallite size with the incorporation of Al in SnO_2: 2% Ni can be attributed to the improvement of the crystalline quality. However, the dislocation density (δ) decreases with the integration of Al in Ni-doped SnO_2 thin films, except Al at 3%, in comparison with the SnO_2 thin film pure. This behavior can be explained by the change of the particle's size (D) with the concentration of aluminum. Indeed, the smaller crystallites allow deposition in relatively large amounts and possibly the appearance of some linear defects (dislocations) and their development throughout the growing structure.

3.2. Optical Properties. The transmission spectra of the Ni- and Al-codoped SnO_2 thin films deposited on the glass substrates by spin coating with a heat treatment temperature of about 500°C are shown in Figure 5. It is a remark clearly that all thin layers have a higher value of the transmittance in the light-visible region and the near-infrared region; it is around the value of 80% and 90%, indicating that Ni- and Al-codoped SnO_2 samples have good optical properties for applications in photovoltaic devices. This behavior is similar to the study of structural and optoelectronic properties of F- and Ni-codoped SnO_2 sprayed thin films, which present a good transmission in the light visible range [29]. It is seen that the transmission depends on the aluminum-doping rate. The high average transmittance in the visible and near-infrared region belongs to 2% Ni- and 1% Al-codoped SnO_2 thin films. Aluminum 5 at. %-doped thin

Table 1: Texture coefficient and lattice parameters of the Al-Ni-codoped SnO_2 thin films (ASTM of SnO_2).

Samples	Texture coefficient		$a = b$ (Å)		c (Å)	
	T_C (110)	T_C (101)	Calculated	ASTM	Calculated	ASTM
SnO_2 pure	1.100	1.095	4.7424	4.7382	3.1925	3.1871
SnO_2: 2% Ni, 0% Al	1.108	1.093	4.7357	4.7382	3.1609	3.1871
SnO_2: 2% Ni, 1% Al	1.058	1.056	4.7224	4.7382	3.1818	3.1871
SnO_2: 2% Ni, 3% Al	1.139	1.104	4.7383	4.7382	3.1955	3.1871
SnO_2: 2% Ni, 5% Al	1.075	1.063	4.7363	4.7382	3.1778	3.1871
SnO_2: 2% Ni, 7% Al	1.064	1.039	4.7154	4.7382	3.1866	3.1871

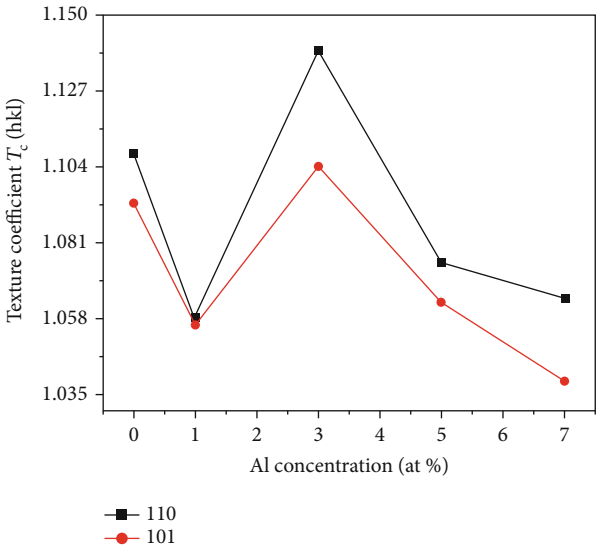

Figure 4: T_C (110) and T_C (101) plotted against the aluminum concentration.

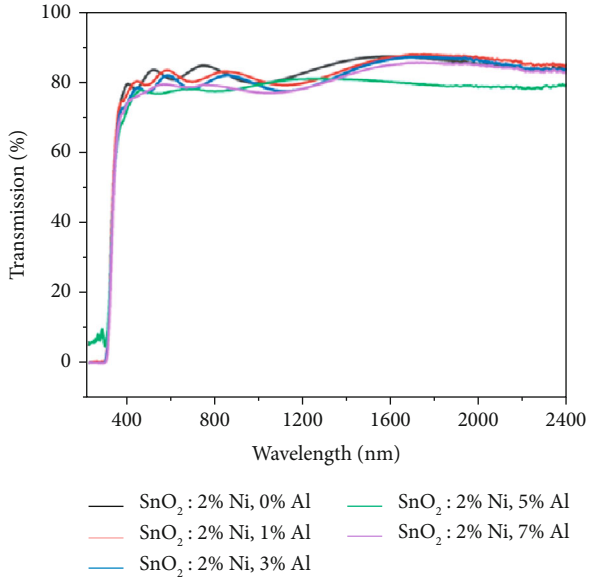

Figure 5: Transmission spectrum of Al-Ni-codoped SnO_2 thin films with Ni = 2 at. % and different Al concentrations (0%, 1%, 3%, 5%, and 7%).

Table 2: Average crystallite size and dislocation density of Al-Ni-codoped SnO_2 thin films prepared at different concentrations of aluminum.

Samples	D (nm)	δ ($\times 10^{-2}$ nm^{-2})
SnO_2 pure	2.51	15.87
SnO_2: 2% Ni; 0% Al	3.95	6.41
SnO_2: 2% Ni; 1% Al	3.39	8.70
SnO_2: 2% Ni; 3% Al	2.37	17.80
SnO_2: 2% Ni; 5% Al	2.96	11.41
SnO_2: 2% Ni; 7% Al	2.96	11.41

films show a slight decrease in transmission compared to undoped in the visible and near-infrared regions. This can be explained by the increase in the optical absorption of the charge carriers, following an increase in their density by the doping effect.

The average transmission of the Al-Ni-codoped SnO_2 thin films decreases with increasing Al concentration. The lower transmittance in the Al-Ni-codoped SnO_2 thin films can be due to the increase in scattering centers (grain boundaries, defects, etc.). It is observed that the SnO_2 films show transparency between 80% and 90% by incorporating an appropriate amount of aluminum, and the transmittance is best at 90%, while Al doping concentration is 1 at. %, the results indicate that a certain doping level of aluminum could improve the transparency of the SnO_2 thin films. When Al doping concentrations exceed 1% at., the transmission decreases; it may be due to the weakening of the crystallization, which could be observed in XRD spectra, increasing the scattering centers for the high concentration of aluminum doping [52, 53], resulting in the enhance of scattering and absorption of light transmission in the thin films. These results of the transmission spectra for SnO_2 thin films are in good agreement with those that are attained from the previous studies [54].

In addition, it is well known that the relation between the absorption coefficient (α) and the incident photon energy ($h\nu$) given by Tauc relation allows us to estimate the optical band gap energy values (E_g) of Ni-doped and Al-Ni-codoped SnO_2 thin films [55]:

$$(\alpha h\nu) = A\left(h\nu - E_g\right)^{1/2}, \quad (6)$$

where A is a constant, α is the absorption coefficient, $h\nu$ is the photon energy, and E_g is the energy gap.

Table 3: The optical band gap for the Al-Ni-codoped SnO_2 thin films.

Samples	SnO_2: 2% Ni; 0% Al	SnO_2: 2% Ni; 1% Al	SnO_2: 2% Ni; 3% Al	SnO_2: 2% Ni; 5% Al	SnO_2: 2% Ni; 7% Al
E_g (eV)	4.084	4.003	3.978	3.800	3.991

The values of the optical band gap of the Al-Ni-codoped SnO_2 thin films are reported in Table 3. The obtained optical band gap values of Ni- and Al-codoped SnO_2 thin layers in the present work are in good agreement with the reported values in the literature [56]. It can be seen that the band gap (E_g) of the SnO_2 deposited thin films decreases when the aluminum-doping rate goes from 1% to 5%. This decrease may be explained by other studies that have reported a similar behavior [57]. Besides, this reduction in band gap energy may be due to the decrease of hole concentration with the increase of Al doping in the codoped SnO_2 thin films. On the other hand, the increase of the band gap energy when the [Al]/[Sn] ratio equals 0.07 has resulted in the reduction of the tail in the valence and conduction band. Finally, the codoping of the SnO_2 thin films by Al and Ni may be used to enhance their electrical conductivity.

The thickness of the Al-Ni-codoped SnO_2 thin layers can be calculated using the transmittance data shown in the interference pattern, according to Swanepoel [11], as follows:

$$d = \frac{\lambda_1 \lambda_2}{2(\lambda_1 n_2 - \lambda_2 n_1)}, \tag{7}$$

where d is the calculated film thickness; λ_1 and λ_2 are the wavelengths at each peak (or valley); and n_1 and n_2 are the refractive index of a thin layer for each wavelength of λ_1 and λ_2.

The refractive index (n) of SnO_2-Ni-Al layers can be calculated using the following equation:

$$\begin{aligned} n &= \sqrt{N + \sqrt{N^2 - n_s^2}}, \\ N &= 2n_s \frac{T_M - T_m}{T_M + T_m} + \frac{n_s^2 + 1}{2}, \end{aligned} \tag{8}$$

where n_s is the refractive index of the substrate (in this case, the glass substrate refractive index = 1.52). T_M and T_m are the maximum and minimum transmittances at a wavelength where the transmittance peak or valley occurs.

Figure 6 shows the thickness of the thin layer of Al-Ni-codoped SnO_2 as a function of aluminum concentration. This thickness of the elaborated films varies from 571 to 694 nm for 2% Ni-doped SnO_2 towards 7% Al and 2% Ni-codoped SnO_2. This variation in the calculated thickness of the films is similar to that obtained experimentally by cross-sectional scanning electron microscopy (SEM), in which the value of the thickness of the thin films varies from 598 to 617 nm. It is clear that the highest thickness is obtained for Al = 7 at. %. Moreover, it is well known that in reality, the thin films, which have the highest thickness, transmit a small amount of light. The thin films were prepared at Al = 7 at. % which have a low value of transmittance

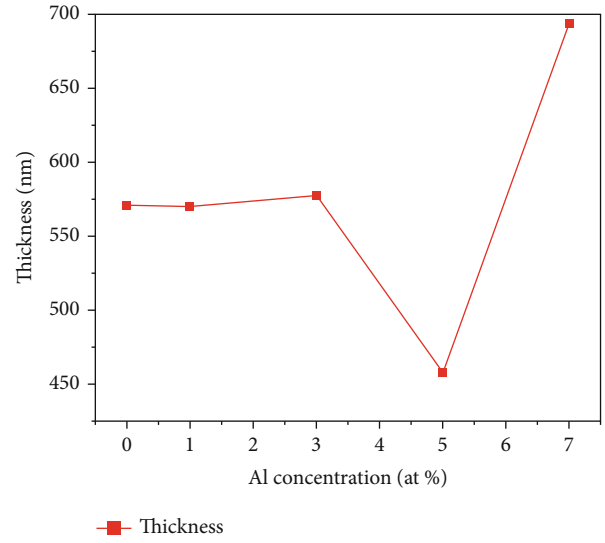

Figure 6: Variation of the thickness of Al-Ni-codoped SnO_2 thin films as a function aluminum-doping rate.

in comparison with the others. This behavior is a good similarity with the other previous work [18]. The increasing thickness of Al-Ni-codoped SnO_2 thin films when the concentration of aluminum goes from 0% to 7% (except 5% Al) can be explained to decrease the transmission of our thin films as indicated in Figure 5.

Urbach energy is defined as an important parameter, which characterizes the material disorder. In the optical energy band gap, the available localized states affect the behavior of the optical transitions. This effect is known as the Urbach tail, indicating the density of localized states of the band edges. In this context, the absorption coefficient of the films showing Urbach tail associated with the disorder in the films is given by the standard relation [58]:

$$\alpha = \alpha_0 \exp(h\nu/E_u), \tag{9}$$

where α_0 is a characteristic parameter of the material, $h\nu$ is the incident photon energy, and E_u presents the Urbach energy, which matches the width of the band located near the conduction or valence bands; from this equation (9), we have explained the optical transition between occupied states in the valance band tail to the unoccupied states of the conduction band [59, 60].

The Urbach tail occurrence is owing to the structural disorder caused by the defects and doping in the films. The Urbach energy values are determined from the slope of ln (α) versus ($h\nu$). The calculated values of E_U are found to be 228.452, 248.945, 251.327, 290.955, and 223.432 meV for 0, 1, 3, 5, and 7 at. % of aluminum, respectively. According to the obtained results, Urbach energy increases with the increase of Al doping concentration introduced in the Ni-

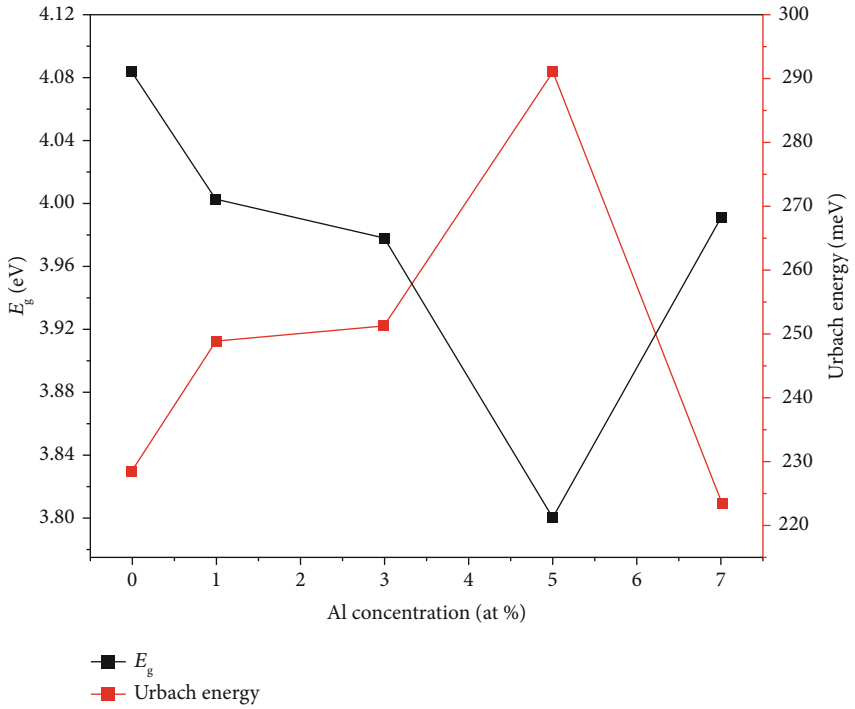

Figure 7: Energy band gap and Urbach energy of Al-Ni-codoped SnO_2 thin films as a function of the aluminum concentration.

doped SnO_2 thin films. There is an inverse relationship between the optical band gap and the Urbach energy, which is a general result [58, 61]. The obtained values of the band gap and Urbach energy were plotted as a function of the aluminum doping concentration as seen in Figure 7. In addition, the increase of broadband tail (Urbach energy) can cause the narrowing of the band gap due to the extension of band tails inside the gap.

The extinction coefficient (K) for Ni-doped and Al-Ni-codoped SnO_2 thin films has been calculated using the values of the absorption coefficient and the wavelength by the following relation [62]:

$$k = \frac{\alpha\lambda}{4\pi}. \tag{10}$$

Figure 8 displays the variation of the extinction coefficient of the Ni-doped and Al-Ni-codoped SnO_2 thin films as a function of wavelength. It is seen that the values of the extinction coefficient decrease in the wavelength range of 275-360 nm and then vary slightly towards longer wavelengths. This increase is attributed to an increase of the absorption coefficient due to the direct electronic transitions at the absorption edge region. However, the decrease in extinction coefficient (k) can be correlated with the decrease of defects and absorption centers in films. It is attractive to see that the transmittance increases slightly with increasing doping of Al, this is due to the decrease of extinction coefficient compared to the increase of refractive index. The reflective index and other dispersion parameters have an important role in identifying the electronic properties of semiconductor materials, and consequently, they consider the main parameters for device design [58]. Therefore, it is a matter of importance to study the effect of aluminum doping on the refractive index of the investigated samples. The refractive indices (n) of Ni-doped and Al-Ni-codoped SnO_2 thin films were determined by the following relation [63]:

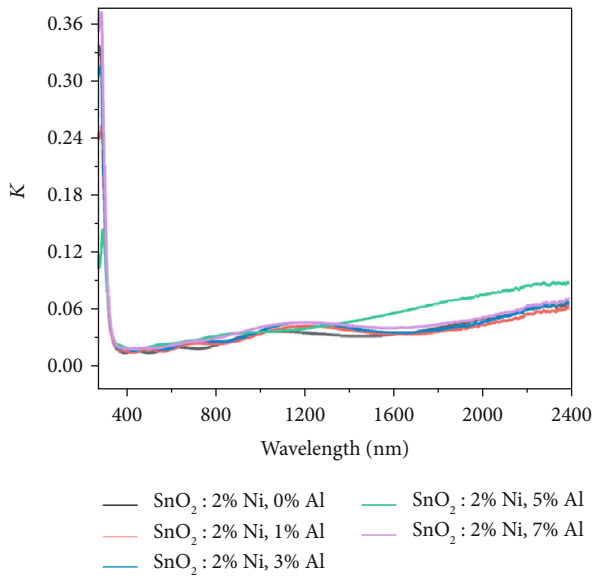

Figure 8: Variation of the extinction coefficient (k) of all Al-Ni-codoped SnO_2 thin films.

$$n = \left(\frac{1+R}{1-R}\right) + \sqrt{\frac{4R}{(1-R)^2} - k^2}, \tag{11}$$

where R is the reflectance and k is the extinction coefficient.

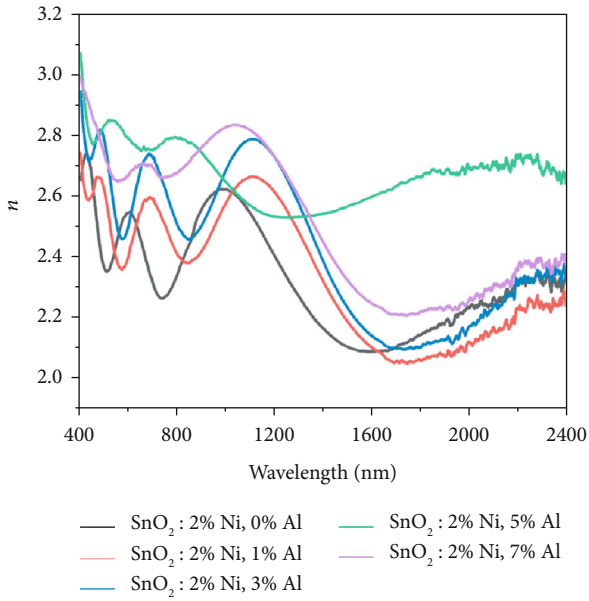

Figure 9: Evolution of the refractive index (n) of Al-Ni-codoped SnO_2 thin films.

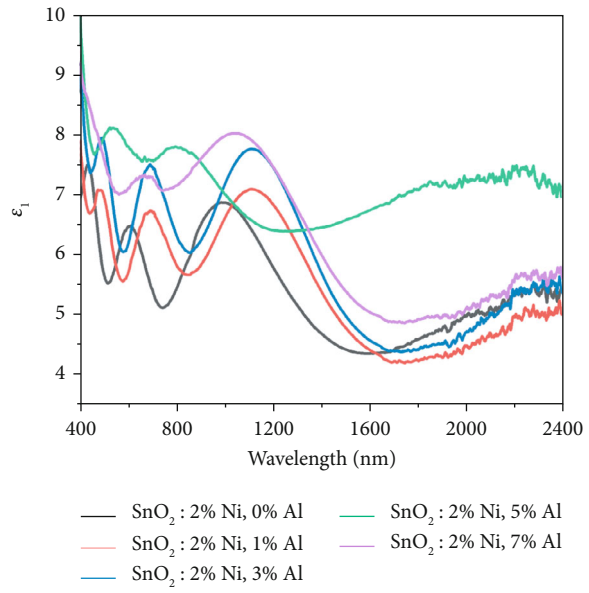

Figure 10: Real part of dielectric constant of Al-Ni-codoped SnO_2 thin films.

Figure 9 illustrates the dependence of refractive index (n) on the wavelength for Ni-doped and Al-Ni-codoped SnO_2 thin films. The refractive index exhibits an oscillatory behavior in the visible and near-IR regions between maximum and minimum values of 2.25 and 2.85, respectively.

The dielectric parameters of Al-Ni-codoped SnO_2 were determinate by using the values of refractive index and extinction coefficient using the following formula [35]:

$$\varepsilon = \varepsilon_1 + i\varepsilon_2, \tag{12}$$

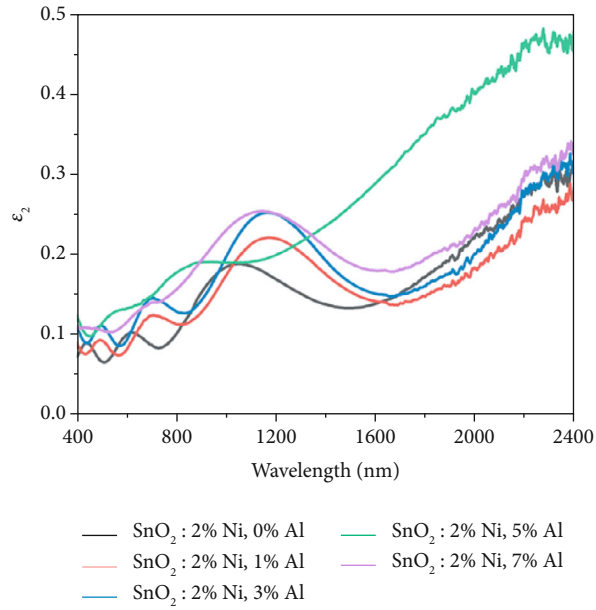

Figure 11: Imaginary part of dielectric constant of Al-Ni-codoped SnO_2 thin films.

where $\varepsilon_1 = n^2 - k^2$ is the real part of the dielectric constant, $\varepsilon_2 = 2nk$ is the imaginary part of the dielectric constant, and n and k are the refractive index and extinction coefficient, respectively. Figures 10 and 11 show the real and imaginary parts of the dielectric constant depending on the wavelength for the Al-Ni-codoped SnO_2 prepared using spin coating technical. The real part of the dielectric constant presents an oscillatory behavior similar to the refractive index n in the visible and near-IR regions between the maximum and minimum values of 5.25 and 8.85, respectively. On the other hand, the imaginary part of the dielectric constant increases when the increasing of wavelength is observed. In addition, as can be seen, the increment of Al concentration in SnO_2: 2% Ni results in an increase of the dielectric parameters.

3.3. Electrical Properties. The resistivity measurement of Ni-doped and Al-Ni-codoped SnO_2 is essential from an application point of view.

The electrical resistivity of the films was measured using the four-probe method at room temperature. The measurement is realized by making four electrical contacts on the sample surface. Two of the probes are used to measure the current, and the other two probes are used to measure the corresponding voltage. The electrical sheet resistance of the thin layers investigated has been measured directly by the device and calculated using the following equation [64, 65]:

$$R_s = \frac{\pi}{\ln(2)} \left(\frac{V}{I}\right). \tag{13}$$

R_s is the sheet resistance, V is the voltage, and I is the current.

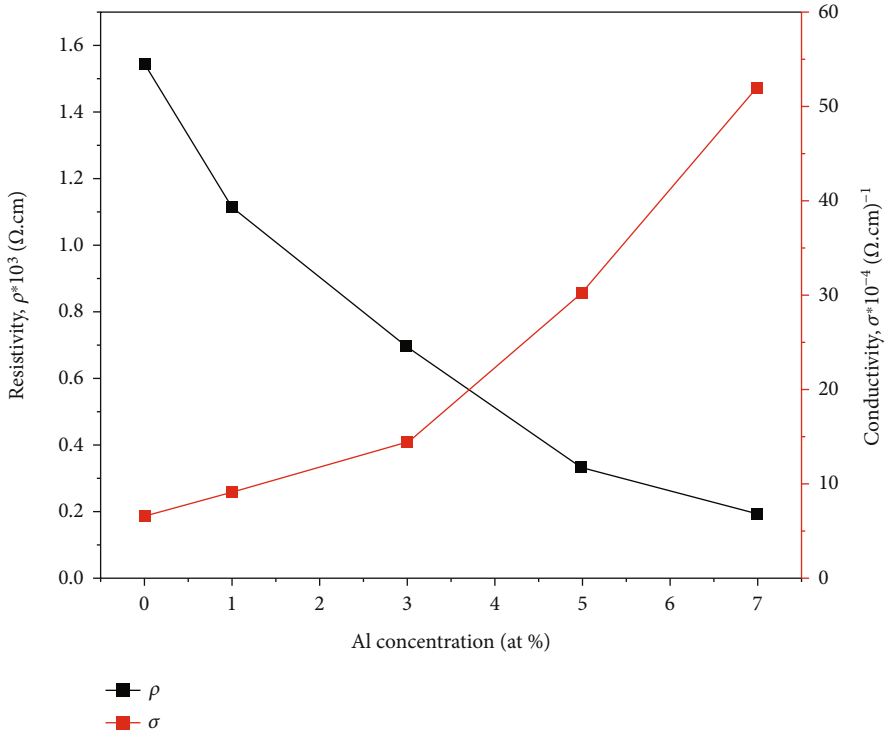

Figure 12: Electrical resistivity and conductivity of Al-Ni-codoped SnO_2 thin films.

The electrical resistivity was estimated using the following equation [66]:

$$\rho = t \times R_s, \tag{14}$$

where "t" is the thickness of the thin films prepared.

From the calculation of the electrical resistivity of the thin films investigated, the electrical conductivity was concluded using the following equation:

$$\sigma = \frac{1}{\rho}. \tag{15}$$

The electrical property measurement substantiated that all our deposited films have the electrical resistivity in an order to 10^3 (ohm·cm). Mariappan et al. for Cd-doped SnO_2 reported a similar value of the electrical resistivity [67]. Figure 12 shows the electrical resistivity and conductivity of the Al-Ni-codoped SnO_2 thin films as a function of the concentration of aluminum. Firstly, we noted that the resistivity of the thin films decreased rapidly from $1.35 \times 10^3\ (\Omega \cdot \mathrm{cm})$ to $0.14 \times 10^3\ (\Omega \cdot \mathrm{cm})$ where the codoping concentration increased from 0 to 7 at. %. The exact same results were reported earlier for F- and Ni-codoped SnO_2 thin films synthesized by chemical spray pyrolysis [18]. Moreover, it is apparent from Figure 12 that the electrical conductivity of the thin films increased with increasing aluminum codoping concentration and reaches a maximum value of $52.15 \times 10^{-4}\ (\Omega \cdot \mathrm{cm})^{-1}$ for the same doping concentration (Al = 7 at. %). It is so that it can be attributed that the Al^{3+} ions were substituted Sn^{4+} and by the increase of the grain size as it was confirmed from the X-ray diffraction.

4. Conclusion

To sum up, the nickel- and aluminum-codoped SnO_2 thin films on a substrate have been prepared by a sol-gel method using the spin coating technique. The XRD study demonstrated that all thin films Ni-doped and Al-Ni-codoped SnO_2 were well crystallized and had a polycrystalline tetragonal structure. X-ray diffraction showed that the thin layers prepared were highly oriented along the (110) peaks. From the optical measurements, it was found that the band gap decreased while the content of Al went from 1% to 5% and increased to 7% Al. The films prepared exhibit a good transmittance between 80% and 90% in the visible and near-infrared regions of the electromagnetic spectrum. The extinction coefficient decreased with the wavelength in the UV region and then varies slightly towards longer wavelengths in the visible and near-infrared regions. The refractive index presented an oscillatory behavior in the visible and near-IR regions. Electrical measurements showed that the electrical resistivity of the thin films studied decreased with increasing aluminum concentration. Also, the electrical conductivity of the thin films investigated increased when Al doping increased. The obtained high optical transmittance of the Al-Ni-codoped SnO_2 thin films that presented a good electrical conductivity around $10^{-4}\ (\Omega \cdot \mathrm{cm})^{-1}$ showed that these thin layers of SnO_2: (Al; Ni) were found to be promising in the various uses of optoelectronic applications, in particular, as window layer in PV solar cells.

Data Availability

Data is available on request.

Conflicts of Interest

The authors declare that they have no conflicts of interest.

Acknowledgments

The National Centre of Scientific and Technological Research, Rabat, Morocco, has supported this research.

References

[1] B. Babu, V. V. N. Harish, R. Koutavarapu, J. Shim, and K. Yoo, "Enhanced visible-light-active photocatalytic performance using CdS nanorods decorated with colloidal SnO_2 quantum dots: Optimization of core-shell nanostructure," *Journal of Industrial and Engineering Chemistry*, vol. 76, pp. 476–487, 2019.

[2] H. J. Jung, R. Koutavarapu, S. Lee, J. H. Kim, H. C. Choi, and M. Y. Choi, "Enhanced photocatalytic degradation of lindane using metal-semiconductor Zn@ZnO and ZnO/Ag nanostructures," *Journal of Environmental Sciences*, vol. 74, pp. 107–115, 2018.

[3] K. Ravindranadh, K. Durga Venkata Prasad, M. C. Rao, and Physics Division, Department of Basic Sciences & Humanities, Chirala Engineering College, Chirala-523 157, India;, "Spectroscopic and luminescent properties of Co^{2+}doped tin oxide thin films by spray pyrolysis," *AIMS Materials Science*, vol. 3, no. 3, pp. 796–807, 2016.

[4] M. C. Rao, R. Koutavarapu, and K. V. Kumar, "Structural and electrochemical properties of ZrO_2 doped PVP-Na^+ based nanocomposite polymer films," *Materials Science in Semiconductor Processing*, vol. 89, pp. 41–50, 2019.

[5] S. J. Lee, H. J. Jung, R. Koutavarapu et al., "ZnO supported Au/Pd bimetallic nanocomposites for plasmon improved photocatalytic activity for methylene blue degradation under visible light irradiation," *Applied Surface Science*, vol. 496, p. 143665, 2019.

[6] Z. Y. Banyamin, P. J. Kelly, G. West, and J. Boardman, "Electrical and optical properties of fluorine doped tin oxide thin films prepared by magnetron sputtering," *Coatings*, vol. 4, no. 4, pp. 732–746, 2014.

[7] D. Miao, Q. Zhao, S. Wu, Z. Wang, X. Zhang, and X. Zhao, "Effect of substrate temperature on the crystal growth orientation of SnO_2:F thin films spray-deposited on glass substrates," *Journal of Non-Crystalline Solids*, vol. 356, no. 44-49, pp. 2557–2561, 2010.

[8] M. Batzill and U. Diebold, "The surface and materials science of tin oxide," *Progress in Surface Science*, vol. 79, no. 2–4, pp. 47–154, 2005.

[9] D. S. Ginley and J. D. Perkins, "Transparent Conductors," in *Handbook of Transparent Conductors*, pp. 1–25, Springer, Boston, MA, 2011.

[10] K. Ellmer, "Past achievements and future challenges in the development of optically transparent electrodes," *Nature Photonics*, vol. 6, no. 12, pp. 809–817, 2012.

[11] R. Swanepoel, "Determination of the thickness and optical constants of amorphous silicon," *Journal of Physics E: Scientific Instruments*, vol. 16, no. 12, pp. 1214–1222, 1983.

[12] M. Gaidi, A. Hajjaji, R. Smirani, B. Bessais, and M. A. El Khakani, "Structure and photoluminescence of ultrathin films of SnO_2 nanoparticles synthesized by means of pulsed laser deposition," *Journal of Applied Physics*, vol. 108, no. 6, p. 63537, 2010.

[13] V. Bilgin, I. Akyuz, E. Ketenci, S. Kose, and F. Atay, "Electrical, structural and surface properties of fluorine doped tin oxide films," *Applied Surface Science*, vol. 256, no. 22, pp. 6586–6591, 2010.

[14] K. Jain, R. P. Pant, and S. T. Lakshmikumar, "Effect of Ni doping on thick film SnO_2 gas sensor," *Sensors and Actuators B: Chemical*, vol. 113, no. 2, pp. 823–829, 2006.

[15] W. Ben Haj Othmen, Z. Ben Hamed, B. Sieber, A. Addad, H. Elhouichet, and R. Boukherroub, "Structural and optical characterization of p-type highly Fe-doped SnO_2 thin films and tunneling transport on SnO_2:Fe/p-Si heterojunction," *Applied Surface Science*, vol. 434, pp. 879–890, 2018.

[16] S. J. Ikhmayies, "The influence of annealing on the optical properties of spray-deposited SnO_2:F thin films," *International Journal of Hydrogen Energy*, vol. 41, no. 29, pp. 12626–12633, 2016.

[17] M. El Jouad, E. M. Bouabdalli, S. Touhtouh, M. Addou, N. Ollier, and B. Sahraoui, "Red luminescence and UV light generation of europium doped zinc oxide thin films for optoelectronic applications," *The European Physical Journal Applied Physics*, vol. 91, no. 1, p. 10501, 2020.

[18] N. Houaidji, M. Ajili, B. Chouial, and N. T. Kamoun, "First investigation of structural and optoelectronic properties of F and Ni co-doped SnO_2 sprayed thin films," *Optik*, vol. 208, p. 164026, 2020.

[19] M. Parthibavarman, B. Renganathan, and D. Sastikumar, "Development of high sensitivity ethanol gas sensor based on Co-doped SnO_2 nanoparticles by microwave irradiation technique," *Current Applied Physics*, vol. 13, no. 7, pp. 1537–1544, 2013.

[20] T. N. Soitah, C. Yang, and L. Sun, "Structural, optical and electrical properties of Fe-doped SnO_2 fabricated by sol-gel dip coating technique," *Materials Science in Semiconductor Processing*, vol. 13, no. 3, pp. 125–131, 2010.

[21] C. Khelifi, A. Attaf, H. Saidi, A. Yahia, M. Dahnoun, and A. Saadi, "Effect of solution flow on the properties of tin dioxide SnO_2 thin films deposited by spray pyrolysis technique," *Optik*, vol. 127, no. 23, pp. 11055–11062, 2016.

[22] X. Liu, S. Chen, M. Li, and X. Wang, "Synthesis and characterization of ferromagnetic cobalt-doped tin dioxide thin films," *Thin Solid Films*, vol. 515, no. 17, pp. 6744–6748, 2007.

[23] M. M. Bagheri-Mohagheghi and M. Shokooh-Saremi, "The electrical, optical, structural and thermoelectrical characterization of n- and p-type cobalt-doped SnO_2 transparent semiconducting films prepared by spray pyrolysis technique," *Physica B: Condensed Matter*, vol. 405, no. 19, pp. 4205–4210, 2010.

[24] X. F. Liu, W. M. Gong, J. Iqbal, B. He, and R. H. Yu, "Structural defects-mediated room-temperature ferromagnetism in Co-doped SnO_2 insulating films," *Thin Solid Films*, vol. 517, no. 21, pp. 6091–6095, 2009.

[25] M. Batzill, J. M. Burst, and U. Diebold, "Pure and cobalt-doped SnO_2(101) films grown by molecular beam epitaxy on Al_2O_3," *Thin Solid Films*, vol. 484, no. 1–2, pp. 132–139, 2005.

[26] L. Zhang, S. Ge, Y. Zuo et al., "Room temperature ferromagnetism in $Sn_{1-x}V_xO_2$ films prepared by sol-gel method," *Journal of Applied Physics*, vol. 104, no. 12, p. 123909, 2008.

[27] C. R. Stefan, M. Elisa, I. C. Vasiliu et al., "Magneto-optical properties of Ce^{3+} and Tb^{3+}-doped silico-phosphate sol-gel thin films," *Applied Surface Science*, vol. 448, pp. 474–480, 2018.

[28] S. Gürakar and T. Serin, "Comprehensive structural analysis and electrical properties of (Cu, Al and In)-doped SnO_2 thin films," *Materials Science and Engineering: B*, vol. 251, p. 114445, 2019.

[29] M. Ajili, M. Castagné, and N. Kamoun Turki, "Spray solution flow rate effect on growth, optoelectronic characteristics and photoluminescence of SnO_2:F thin films for photovoltaic application," *Optik*, vol. 126, no. 7-8, pp. 708–714, 2015.

[30] H. Han, S. Kment, F. Karlicky et al., "Sb-doped SnO2 Nanorods underlayer effect to the α-Fe2O3 Nanorods sheathed with TiO2 for enhanced photoelectrochemical water splitting," *Small*, vol. 14, no. 19, 2018.

[31] A. E. Hassanien, H. M. Hashem, G. Kamel et al., "Performance of transparent conducting fluorine-doped tin oxide films for applications in energy efficient devices," *International Journal of Thin Film Science and Technology*, vol. 5, no. 1, 2016.

[32] A. Abdelkrim, S. Rahmane, O. Abdelouahab, N. Abdelmalek, and G. Brahim, "Effect of solution concentration on the structural, optical and electrical properties of SnO_2 thin films prepared by spray pyrolysis," *Optik*, vol. 127, no. 5, pp. 2653–2658, 2016.

[33] M. M. Bagheri-Mohagheghi, N. Shahtahmasebi, M. R. Alinejad, A. Youssefi, and M. Shokooh-Saremi, "Fe-doped SnO_2 transparent semi-conducting thin films deposited by spray pyrolysis technique: thermoelectric and p-type conductivity properties," *Solid State Sciences*, vol. 11, no. 1, pp. 233–239, 2009.

[34] B. Benrabah, A. Bouaza, S. Hamzaoui, and A. Dehbi, "Sol-gel preparation and characterization of antimony doped tin oxide (ATO) powders and thin films," *The European Physical Journal Applied Physics*, vol. 48, no. 3, p. 30301, 2009.

[35] M. Girtan, G. I. Rusu, G. G. Rusu, and S. Gurlui, "Influence of oxidation conditions on the properties of indium oxide thin films," *Applied Surface Science*, vol. 162-163, pp. 492–498, 2000.

[36] M. Ajili, M. Castagné, and N. K. Turki, "Study on the doping effect of Sn-doped ZnO thin films," *Superlattices and Microstructures*, vol. 53, no. 1, pp. 213–222, 2013.

[37] M. Abd-Lefdil, R. Diaz, H. Bihri, M. Ait Aouaj, and F. Rueda, "Preparation and characterization of sprayed FTO thin films," *The European Physical Journal Applied Physics*, vol. 38, no. 3, pp. 217–219, 2007.

[38] P. Srinivasa Subbarao, Y. Aparna, and K. L. Chitturi, "Synthesis and characterization of Ni doped SnO_2 nanoparticles by sol-gel method for novel applications," *Materials Today: Proceedings*, vol. 26, pp. 1676–1680, 2020.

[39] A. S. Ahmed, M. Muhamed Shafeeq, M. L. Singla, S. Tabassum, A. H. Naqvi, and A. Azam, "Band gap narrowing and fluorescence properties of nickel doped SnO_2 nanoparticles," *Journal of Luminescence*, vol. 131, no. 1, pp. 1–6, 2011.

[40] F. H. Aragón, J. A. H. Coaquira, L. Villegas-Lelovsky et al., "Evolution of the doping regimes in the Al-doped SnO_2 nanoparticles prepared by a polymer precursor method," *Journal of Physics: Condensed Matter*, vol. 27, no. 9, p. 095301, 2015.

[41] M. M. Bagheri-Mohagheghi and M. Shokooh-Saremi, "The influence of Al doping on the electrical, optical and structural properties of SnO2 transparent conducting films deposited by the spray pyrolysis technique," *Journal of Physics D: Applied Physics*, vol. 37, no. 8, pp. 1248–1253, 2004.

[42] R. Rivera, F. Marcillo, W. Chamba, P. Puchaicela, and A. Stashans, "SnO_2 physical and chemical properties due to the impurity doping," *Lecture Notes in Engineering and Computer Science*, vol. 2203, 2013.

[43] E. Elangovan, M. P. Singh, and K. Ramamurthi, "Studies on structural and electrical properties of spray deposited SnO_2:F thin films as a function of film thickness," *Materials Science and Engineering B*, vol. 113, no. 2, pp. 143–148, 2004.

[44] T. Garmim, S. Chahib, L. Soussi et al., "Optical, electrical and electronic properties of SnS thin films deposited by sol gel spin coating technique for photovoltaic applications," *Journal of Materials Science: Materials in Electronics*, vol. 31, no. 23, pp. 20730–20741, 2020.

[45] A. V. Moholkar, S. M. Pawar, K. Y. Rajpure, S. N. Almari, P. S. Patil, and C. H. Bhosale, "Solvent-dependent growth of sprayed FTO thin films with mat-like morphology," *Solar Energy Materials & Solar Cells*, vol. 92, no. 11, pp. 1439–1444, 2008.

[46] A. Ben Haoua, A. Rahal, and B. . Ben Haoua, "Caractérisations structurale, optique et electrique des couches minces du SnO_2, non dopé et dopé au lithium, elaborées par spray ultrasonique," *Annals of science and technology*, vol. 7, no. 1, pp. 6–11, 2015.

[47] N. Benkhettou, D. Rached, B. Soudini, and M. Driz, "High-pressure stability and structural properties of CdS and CdSe," *physica status solidi (b)*, vol. 241, no. 1, pp. 101–107, 2004.

[48] S. Chandra, G. George, K. Ravichandran, and K. Thirumurugan, "Influence of simultaneous cationic (Mn) and anionic (F) doping on the magnetic and certain other properties of SnO_2 thin films," *Surfaces and Interfaces*, vol. 7, pp. 39–46, 2017.

[49] B. S. Rao, B. R. Kumar, V. R. Reddy, and T. S. Rao, "X-ray diffraction and transmission electron microscopy studies on nickel doped CdS nanoparticles," *Digest Journal of Nanomaterials and Biostructures*, vol. 6, no. 4, 2011.

[50] T. Garmim, L. Soussi, A. Louardi et al., "Structural and optical characterization of sprayed Mg and Ni co-doped CdS thin films for photovoltaic applications," *IOP Conference Series: Materials Science and Engineering*, vol. 948, no. 1, 2020.

[51] K. Pakiyaraj, V. Kirthika, and K. Karthik, "Effect of annealing on the structural, morphological, optical and electrical properties of Al-Zn co-doped SnO2 thin films," *Materials Research Innovations*, vol. 24, no. 4, pp. 193–201, 2020.

[52] N. N. K. Reddy, H. S. Akkera, M. C. Sekhar, and S. H. Park, "Zr-doped SnO_2 thin films synthesized by spray pyrolysis technique for barrier layers in solar cells," *Applied Physics A*, vol. 123, no. 12, 2017.

[53] J. Mazloom, F. E. Ghodsi, and M. Gholami, "Fiber-like stripe ATO (SnO_2:Sb) nanostructured thin films grown by sol-gel method: optical, topographical and electrical properties," *Journal of Alloys and Compounds*, vol. 579, pp. 384–393, 2013.

[54] S. Sambasivam, P. S. Maram, C. V. V. Muralee Gopi, and I. M. Obaidat, "Effect of erbium on the structural, morphological, and optical properties of SnO_2 thin films deposited by spray pyrolysis," *Optik*, vol. 202, p. 163596, 2020.

[55] J. Tauc, R. Grigorovici, and A. Vancu, "Optical properties and electronic structure of amorphous germanium," *physica status solidi (b)*, vol. 15, no. 2, 1966.

[56] O. Erken, O. M. Ozkendir, M. Gunes, E. Harputlu, C. Ulutas, and C. Gumus, "A study of the electronic and physical properties of SnO_2 thin films as a function of substrate temperature," *Ceramics International*, vol. 45, no. 15, pp. 19086–19092, 2019.

[57] T. M. Al-Saadi, B. H. Hussein, A. B. Hasan, and A. A. Shehab, "Study the Structural and Optical Properties of Cr doped SnO_2 Nanoparticles Synthesized by Sol-Gel Method," *Energy Procedia*, vol. 157, pp. 457–465, 2019.

[58] F. Urbach, "The long-wavelength edge of photographic sensitivity and of the electronic absorption of solids," *Physical Review*, vol. 92, no. 5, p. 1324, 1953.

[59] M. Yilmaz, "A function of external doping: characteristics of inorganic nanostructure based diode," *Ceramics International*, vol. 45, no. 1, pp. 665–673, 2019.

[60] M. Yilmaz, D. Tatar, E. Sonmez, C. Cirak, S. Aydogan, and R. Gunturkun, "Investigation of structural, morphological, optical, and electrical properties of Al doped ZnO thin films via spin coating technique," *Synthesis and Reactivity in Inorganic, Metal-Organic, and Nano-Metal Chemistry*, vol. 46, no. 4, pp. 489–494, 2016.

[61] M. Yilmaz, "Investigation of characteristics of ZnO:Ga nanocrystalline thin films with varying dopant content," *Materials Science in Semiconductor Processing*, vol. 40, pp. 99–106, 2015.

[62] A. S. Hassanien and A. A. Akl, "Influence of composition on optical and dispersion parameters of thermally evaporated non-crystalline $Cd_{50}S_{50-x}Se_x$ thin films," *Journal of Alloys and Compounds*, vol. 648, pp. 280–290, 2015.

[63] R. M. Abdelhameed and I. M. El Radaf, "Self-cleaning lanthanum doped cadmium sulfide thin films and linear/nonlinear optical properties," *Materials Research Express*, vol. 5, no. 6, 2018.

[64] Z. Essalhi, B. Hartiti, A. Lfakir, B. Mari, and P. Thevenin, "Optoelectronics properties of TiO_2:Cu thin films obtained by sol gel method," *Optical and Quantum Electronics*, vol. 49, no. 9, 2017.

[65] T. Garmim, E. Bouabdalli, L. Soussi et al., "Opto-electrical properties of ni and mg co-doped cds thin films prepared by spin coating technique," *Physica Scripta*, vol. 96, no. 4, p. 045813, 2021.

[66] A. Ziti, B. Hartiti, H. Labrim et al., "Study of kesterite CZTS thin films deposited by spin coating technique for photovoltaic applications," *Superlattices and Microstructures*, vol. 127, pp. 191–200, 2019.

[67] R. Mariappan, V. Ponnuswamy, P. Suresh, R. Suresh, M. Ragavendar, and C. Sankar, "Deposition and characterization of pure and Cd doped SnO_2 thin films by the nebulizer spray pyrolysis (NSP) technique," *Materials Science in Semiconductor Processing*, vol. 16, no. 3, pp. 825–832, 2013.